Journal of Advanced Marine Engineering and Technology, Vol. 45, No. 6, pp. 356~362, 2021
J. Advanced Marine Engineering and Technology (JAMET)
https://doi.org/10.5916/jamet.2021.45.6.356

ISSN 2234-7925 (Print)
ISSN 2765-4796 (Online)
Original Paper

Effect of bifilm defects on Microstructure and Tensile properties of A356 secondary alloy for the recycling of machining chip scrap

Minhye Kang[1] · Eunkyung Lee[†]

(Received October 6, 2021 ; Revised November 2, 2021 ; Accepted December 6, 2021)

Abstract: With the growing demand for aluminum alloys, interest in recycling aluminum is increasing due to economic and environmental reasons. In order to evaluate the recyclability of machining chip scrap, microstructural analysis and tensile tests of A356 cast alloys with different scrap fraction of 0, 20, 40, 60, 80, and 100% were conducted. The secondary dendrite arm spacing increased from 26.21 to 36.34 μm as the scrap content increased. The microstructure comprised an α-Al matrix, eutectic Si, α-Al_8Fe_2Si, β-Al_5FeSi, and π-$Al_8Mg_3FeSi_6$, which possess similar microstructures to those of commercial A356 cast alloys. The test results showed that the size and number of pores increased with the increasing scrap content. When the scrap content was higher than 40%, the pore area fraction increased significantly up to 5.97% for 100% scrap. It was shown that increasing the scrap content decreased the average tensile strength, yield strength, and elongation to 94.34 MPa, 72.10 MPa, and 5.22%, respectively. The porosities and tensile strengths of A356 alloy without scrap content were considered to have similar values to 20% scrap contents. Pores were found on the fracture surfaces under all the conditions.

Keywords: A356, Recycling, Scrap, Tensile properties, Microstructure, Bifilm defects

1. Introduction

Aluminum alloys have received wide attention as lightweight materials owing to global eco-friendly policies, such as CO_2 emission regulations in the European Union and environmental regulations of the International Maritime Organization **[1]-[3]**. With the increasing demand for aluminum alloys in the automotive, aerospace, and other industries, the interest in recycling aluminum is increasing due to economic and environmental reasons **[4]-[5]**. The energy required to produce aluminum from bauxite is approximately 30,000 kJ/kg, while the energy required in the remelting process of aluminum scrap is approximately 960 kJ/kg, which is only 5% of the primary production consumption **[6]-[7]**. Therefore, the amount of hazardous substances and emissions from the aluminum production process can be reduced, which is advantageous for environmental protection.

With the widespread use of aluminum alloys, the amount of scrap produced during the manufacturing of aluminum components is steadily increasing. Approximately 15% of materials are lost during the manufacturing process, and all of the waste aluminum is scrapped **[8]**.

Secondary generated aluminum scraps can be classified as: riser-scraps, dross, defective products produced during the casting process, and machining chips in the precision manufacturing process. Among them, machining chips generated during the shaving process have approximately 10% of the cutting fluid on the surface, which causes environmental pollution when discarded **[9]**. However, machining chips have a relatively pure composition with a low impurity content, so are considered a valuable recycling resource after the removal of the cutting fluid **[10]**.

Currently, the industry recycles machining chip scraps to manufacture secondary aluminum alloys. However, the analysis of the properties and problems based on scrap input fraction are limited, which is also selected based on experience **[5]**. Process optimization and basic research on the specific properties of alloys are necessary for the production of secondary aluminum. Therefore, the evaluation of changes in the microstructure and mechanical properties of secondary aluminum alloys manufactured with different amounts of scrap should be conducted.

† Corresponding Author (ORCID: https://orcid.org/0000-0003-0723-8524): Assistant Professor, Interdisciplinary Major of Maritime AI convergence, Department of Ocean Advanced Materials Convergence Engineering, 727, Taejong-ro, Yeongdo-gu, Busan 49112, Korea, E-mail: elee@kmou.ac.kr, Tel: 051-410-4353

1 M. S. Candidate, Interdisciplinary Major of Maritime AI convergence, Department of Ocean Advanced Materials Convergence Engineering, Korea Maritime & Ocean University, E-mail: minhye1228@naver.com, Tel: 051-410-4955

Table 1: Chemical composition of A356 alloy in ASTM and used (wt. %)

Scrap ratio	Si	Mg	Fe	Ti	Mn	Zn	Cu	Al
A356	6.5~7.5	0.25~0.45	≤0.2	≤0.2	≤0.1	≤0.1	≤0.1	Rem.
0%	8.85	0.28	0.137	0.11	0.094	0.013	0.028	Rem.
20%	8.08	0.30	0.153	0.099	0.028	0.014	0.032	Rem.
40%	7.84	0.42	0.155	0.106	0.031	0.015	0.031	Rem.
60%	8.11	0.16	0.154	0.127	0.019	0.017	0.031	Rem.
80%	8.88	0.20	0.176	0.121	0.019	0.018	0.034	Rem.
100%	8.20	0.16	0.172	0.109	0.018	0.019	0.033	Rem.

Because of the oxide layer that forms on the machining chip scrap with small flat shapes, it is highly likely that a certain quantity of oxides will be entrained into the molten metal during the casting process **[11]-[12]**. Bifilm, produced by the entrainment of the oxide film, is one of the common casting defects in aluminum cast alloys, providing nucleation sites for porosity and brittle intermetallic compounds, such as β-Al_5FeSi **[13]-[15]**. Therefore, it is expected that the formation of bifilm from the oxide film will inevitably lead to the degradation of the mechanical properties.
In order to improve the reliability and economical application of aluminum recycling components, it is imperative to consider the changes in the properties of alloys based on the scrap fraction. This study investigated the recyclability of high-purity machining chip scraps generated during the manufacturing of automotive components.

2. Experimental procedure

2.1 Materials

A356 cast alloy with different addition of scrap (0, 20, 40, 60, 80, 100 %) were investigated in this study to determine the effect of scrap content on the tensile properties. The composition of A356 cast alloy with different addition of scrap and A356 alloy in ASTM were shown in **Table 1**. Scrap used in the study has same chemical composition as A356 primary alloy and produced in the shaving process of precision manufacturing process. Before the casting process, cleaning with surfactants and heat treatment at 500 °C for 3 hours was conducted to eliminate the cutting fluids on the surfaces of machining chip. Aluminum scraps were re-melted in graphite crucible furnace with A356 primary ingots at 750 °C to obtained molten aluminum and injected into mold.

2.2 Tensile test

In order to evaluate the tensile properties A356 cast alloy with different addition of scrap, sub-sized test specimens based on ASTM E8 were manufactured and tensile tests were conducted. The cross-head speed was set to 1 mm/min, and the test was repeated five times per experimental condition using UNIVERSAL TEST MACHINE KDMT-156.

2.3 Reduced pressure test

Reduced pressure test (RPT) was performed to evaluate the melt quality. RPT applies a much lower pressure than atmospheric pressure to solidify the sample and enlarge the hydrogen in porosity inside the sample by nearly 100 times. This study conducted reduced pressure test to measure porosity area fraction. RPT samples were solidified at 0.8 atm for 240 seconds.

2.4 Microstructure analysis

JmatPro® software was used to analyze the thermodynamics of phase formation in A356 alloys. It was calculated based on the A356 chemical composition in ASTM, the temperature range was set from 25 °C to 750 °C. The phases formed in the simulation were compared with those actually shown in the A356 cast alloy with scraps.

All test specimens were polished from 200 to 2400-grit silicon carbide paper, 0.25 μm diamond suspension, and 0.04 μm colloidal suspension. Microstructure and fracture surfaces were observed using Optical microscope (OM, eclipse LV150N, Nikon) and field emission scanning electron microscopy (FE-SEM, MIRA3, Tescan) with Energy-dispersive X-ray spectroscopy (EDS, EDAX).

3. Results and Discussion

3.1 Microstructure

Figure 1 showed the microstructure of A356 cast alloy with the different addition of scrap using optical microscope. As shown in **Figure 2**, SDAS was observed to increase with scrap content increased. A356 cast alloy without scrap addition had smallest SDAS value of 26.21 μm. On the other hand, A356 alloy with 100 % scrap had the largest value of 36.34 μm, showing a difference of approximately 10 μm compared to the condition without scrap addition.

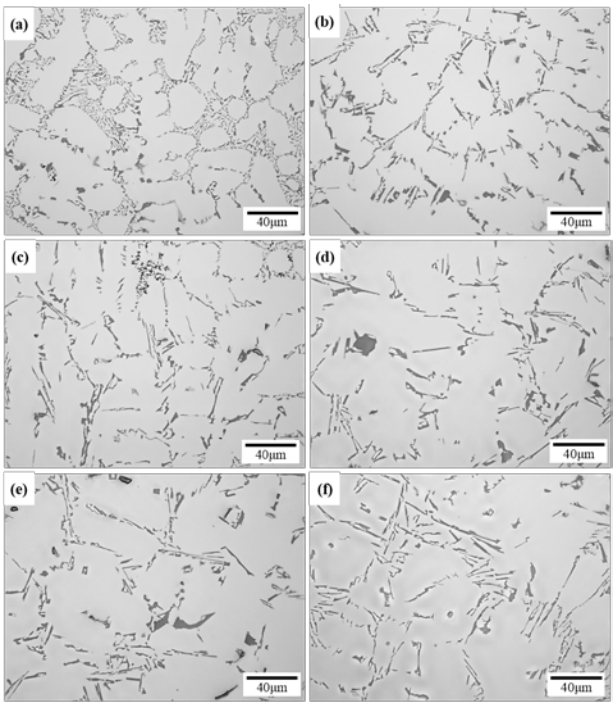

Figure 1: The microstructure of A356 cast alloy (a) without scrap, with the addition of (b) 20 % scrap, (c) 40 % scrap, (d) 60 % scrap, (e) 80% scrap, (f) 100 % scrap

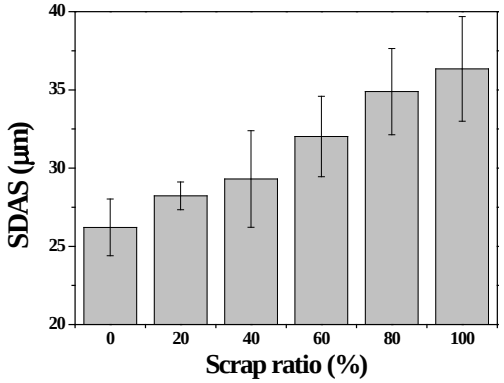

Figure 2: The results of secondary dendrite arm spacing measurements of A356 cast alloy

Figure 3 showed the result of thermodynamic simulation using JmatPro® software. As shown in **Figure 3(a)**, α-Al matrix starts to form around 640 °C and eutectic Si phase begins to form around 560 °C. **Figure 3(b)** showed that the amount of α-Al_8Fe_2Si is estimated to be the highest based on the amount produced, and then decreases in the order of $Al_5Cu_2Mg_8Si_6$, β-Al_5FeSi, Mg_2Si, and Al_3M(M = transition element). Unlike the results of the analytical program, it is generally known that A356 alloys have no $Al_5Cu_2Mg_8Si_6$ phases with low Cu content of lower than 0.1 **[16]-[17]**. π-Al_8Mg_3FeSi appears to be produced near 500 °C, but dissipated at all around 400 °C.

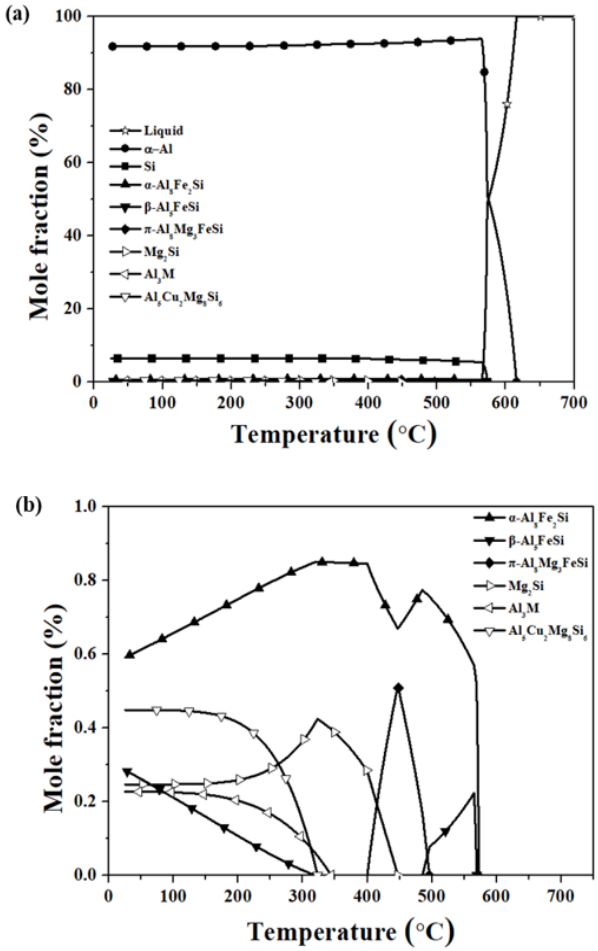

Figure 3: (a) Mole fraction of different phases as a temperature function in the Al-7Si-0.3Mg-0.2Fe-0.1Ti-0.1Mn-0.1Zn-0.1Cu system. (b) Detail view except for Liquid, α-Al and Si

Figure 4 shows the microstructures, and **Table 2** shows the intermetallic compound composition determined using FE-SEM and EDS. The microstructures observed were composed of an α-Al matrix, eutectic Si, β-Al_5FeSi, π-$Al_8Mg_3FeSi_6$, and α-Al_8Fe_2Si. The composition of the scrap content in **Table 1** is thought to have no significant effect on the formation of intermetallic compounds. There were no significant differences in the intermetallic compounds of the A356 cast alloy with different scrap fractions. The β-Al_5FeSi and α-Al_8Fe_2Si observed in the microstructures are consistent with the thermodynamic simulation results. Meanwhile, in the case of π-$Al_8Mg_3FeSi_6$, the thermodynamic analysis of the A356 alloy showed that it was extinguished near 400 °C, but it was observed in the SEM analysis. When the Cu content was very low, the Al-Si-Mg system alloys form π-

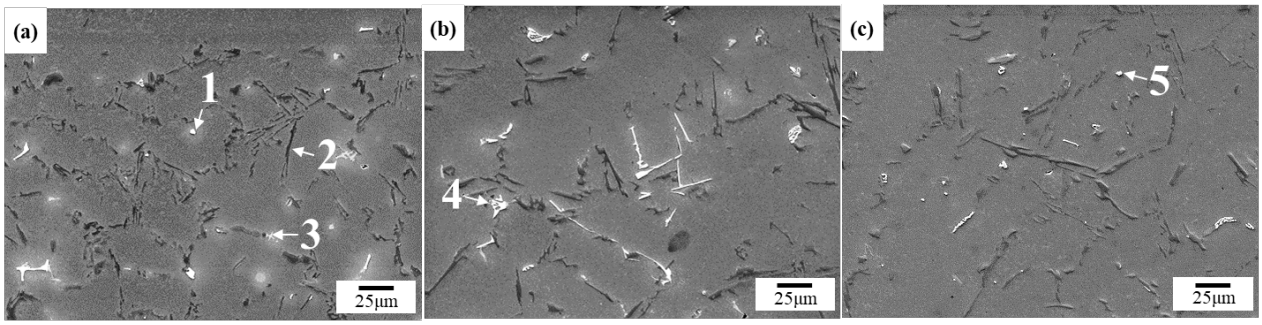

Figure 4: SEM microstructure of the A356 cast alloy with the addition of scrap, and the numbers correspond to the qualitative analysis in **Table 2**

Table 2: Qualitative analysis of the intermetallic phase corresponding to the points in **Figure 4**

Number	Composition (at. %)				Interfacial Component
	Al	Si	Fe	Mg	
1	74.22	10.78	14.99	-	β-Al_5FeSi
2	07.21	92.29	-	-	Eutectic Si
3	50.50	26.32	06.30	16.88	π-$Al_8Mg_3FeSi_6$
4	71.69	10.93	17.38	-	α-Al_8Fe_2Si
5	67.87	15.56	16.63	-	β-Al_5FeSi

$Al_8Mg_3FeSi_6$ instead of Al_2Cu or $Al_5Cu_2Mg_8Si_6$ **[18]**. The intermetallic compounds in all conditions were identified to be the same as those of the commercial A356 cast alloy.

3.2 Porosity Analysis

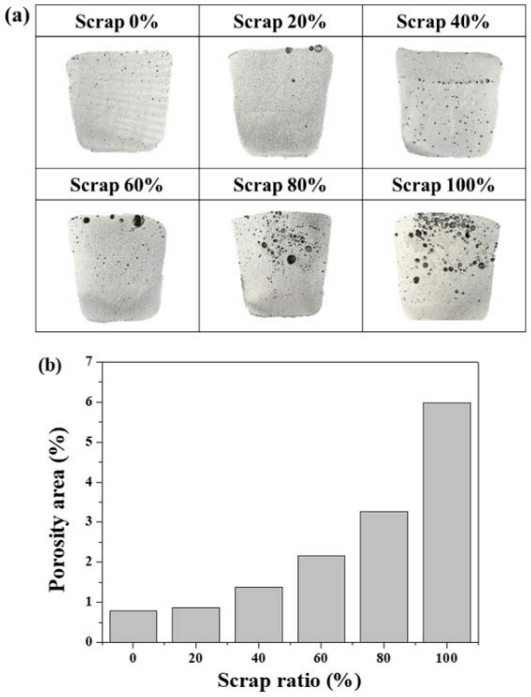

Figure 5: (a) The picture of reduced pressure test samples of A356 cast alloys, (b) the results of porosity area fraction measurements of A356 cast alloy with the addition of scrap

The bifilms, produced by the entrainment of oxide, are nucleation sites for pores that allow the dissolved hydrogen to escape into the gap between the double oxide films **[19]**. As a result, with an increase in the oxide film entrainment quantity, the amount of bifilm produced also increases, resulting in an increased porosity. This phenomenon is illustrated in **Figure 5**, which shows a sample subjected to an RPT and the porosity area fraction for different scrap ratios.

A higher scrap content was observed to increase the size and number of pores. Without scrap addition, a 0.78% porosity area fraction was found, and it increased to 0.86% as the scrap content increased to 20%. The difference in the porosity area fraction between the case of no scrap addition and 20% scrap addition is 0.08% and is considered very small. When the scrap content increased to more than 40%, the porosity increased significantly, measuring 5.97% under scrap-only casting conditions.

3.3 Tensile properties

Figure 6 shows tensile test results of A356 cast alloy with different addition of scrap. As scrap content increased, the average tensile strength, average yield strength, and average elongation tended to gradually decrease. The highest average tensile strength is 140.16 MPa, which is shown in the condition of scrap 20 % addition and has a small difference of about 8 MPa compared to the no scrap addition. As mentioned above, the two conditions showed a slight difference of 0.08 % when measuring

the porosity area fraction, with relatively low porosity quantity compared to other conditions. Therefore, when the scrap content is less than 20 %, the amount of pores produced is similar to the condition without scraps, and the tensile properties are not significantly different. The average elongation was also found to have the highest value in a test piece with a scrap content of 20 %, as was the tensile strength. For the mean yield strength, the highest value was 103.15 MPa under the condition of no scrap addition, and then slowly decreased to an average value of 72.10 MPa under the condition of 100 % scrap content. When scrap content is greater than 40%, tensile properties have been deteriorated due to a rapid increase in porosity area fraction, but it is also believed that increased SDAS will have an effect on tensile properties.

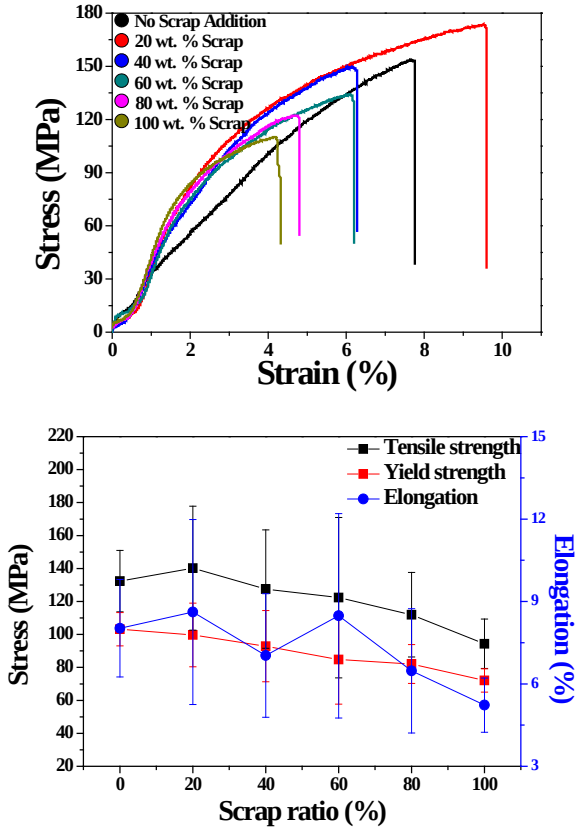

Figure 6: (a) Stress-strain curves for A356 cast alloy with different addition of scrap, (b)Tensile strength, yield strength, and elongation of A356 cast alloy with the addition of scrap

3.4 Fractography

The results of the analysis of the fracture surfaces of the tensile test specimens of A356 cast alloy with different addition of scrap are shown in **Figure 7**. Dimple which is the trace of ductile fracture and porosities were observed in all conditions of fracture surfaces. Thus, it can be seen that the porosities acted as a stress concentrator, affecting the propagation of the crack. Under the condition of casting with 100 % scrap, traces of very large pores were observed on the fracture surfaces. The oxide film on the scrap surface may have caused the formation of Bifilm and increased the amount of hydrogen gas incorporation, resulting in a sharp decrease in tensile strength.

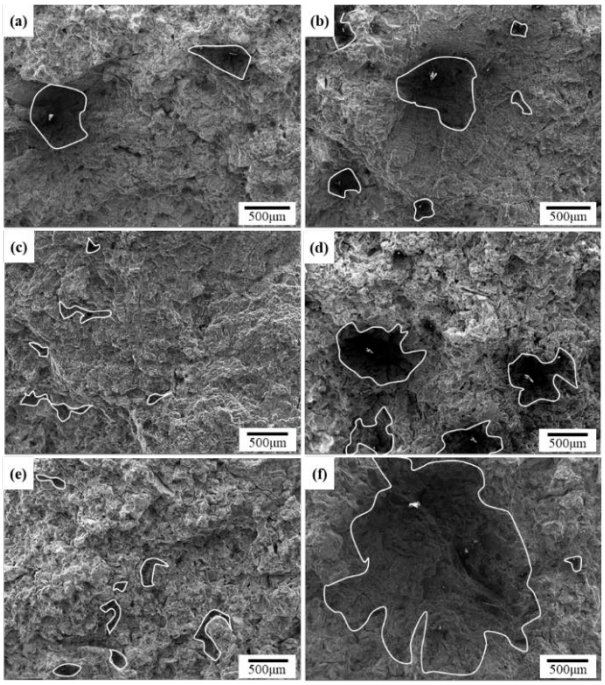

Figure 7: Image of porosity(highlighted by white line) on fracture surfaces: A356 cast alloy (a) without scrap, with the addition of (b) 20 % scrap, (c) 40 % scrap, (d) 60 % scrap, (e) 80 % scrap, (f) 100 % scrap

An oxide analysis of the porosity surfaces of the fracture surface using FE-SEM and EDS is shown in **Figure 8**. **Figure 8(a)** is a microstructure of a porosity on fracture surface, which is thought to be gas porosity with no dendrite observed. The gas porosity has been reported to have a relatively smooth surface compared to the shrinkage porosity by inflating and forming the gap as hydrogen gas escapes through the wetted side of the bifilm **[20]**. Analysis of spherical particles shown in **Figure 8(b)** suggests that MgO was produced. Al_2O_3 forming bifilm combines with Mg over time when alloys in liquid phase and transformed to $MgAl_2O_4$, which can then undergo phase transformation with MgO **[21]**. **Figure 8(d)** is a dendrite observed inside the pores. Given that dendrite is observed on the surface of the pores, it is believed that liquid Al is cooled and contracted, resulting in shrinkage porosity. As the solidification contraction of the

aluminum progresses, the volume of the bifilm expands rapidly, the oxide film on the surface is torn, and it is buried in the dendrite side **[22]**. As shown in **Figure 8(e)**, traces of oxide film were observed on the dendrite surface of the shrinkage porosity.

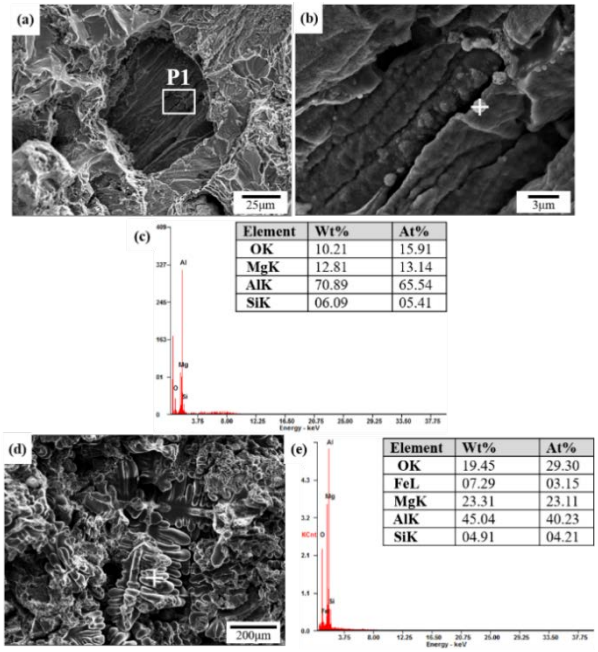

Figure 8: Oxides on the porosity surface: (a) porosity on fracture surface, (b) magnification of the P1 in (a), (c) qualitative analysis of the intermetallic phase corresponding to the point in (b), (d) dendrites of shrinkage porosity surface, (e) qualitative analysis of the intermetallic phase corresponding to the point in (d).

4. Conclusion

A356 cast alloy with different addition of scrap (0, 20, 40, 60, 80, 100 %) were investigated in this study to determine the effect of scrap content on the tensile properties. The microstructures are consisted of α-Al matrix, eutectic Si, α-Al_8Fe_2Si, β-Al_5FeSi and π-$Al_8Mg_3FeSi_6$. Significant difference in microstructure wasn't observed, but porosity area fraction increased with scrap contents increasing. The maximum and minimum value of porosity area fraction was 0.78 % and 5.97 % under 0% and 100 % scrap casting condition, respectively. The difference of porosity area fraction between scrap 0 % and 20% is 0.08 % which is not a great value. The tensile strength decreased from 140.16 MPa to 72.10 MPa as the scrap content increased from 20 % to 100 %. Tensile strength under the condition without scrap addition was 132.33 MPa which was slightly decreased from the value of condition without scrap addition. Adding up to 20 % of scrap content, it was considered that the amount of porosities and tensile strength have similar values compared to A356 alloy without addition of scrap. From the fractography, there were porosities and dimple which is the evidence of ductile fracture. EDS analysis of fracture surfaces showed that the oxygen concentration inside the porosity measured, which suggests the bifilm covering the inner surface of gas porosity and shrinkage porosity.

Acknowledgement

This work was supported by the Busan Techno-Park grant funded by the Busan Metropolitan city (Title: 생산성 향상(50%이상)을 위한 전기차 제너레이터 모터 하우징 금형 기술 개발 (in Korean)) . Also, this work was supported by the Korea Institute for Advancement of Technology (KIAT) grant funded by the Korea Government (MOTIE) (P0008763, The Competency Development Program for Industry Specialist).

Author Contributions

Conceptualization, M. H. Kang and E. K. Lee; Methodology, M. H. Kang; Software, M. H. Kang; Validation, M. H. Kang and E. K. Lee; Formal Analysis, M. H. Kang; Investigation, M. H. Kang; Resources, M. H. Kang; Data Curation, M. H. Kang; Writing—Original Draft Preparation, M. H. Kang; Writing—Review & Editing, E. K. Lee; Visualization, M. H. Kang; Supervision, E. K. Lee; Project Administration, E. K. Lee; Funding Acquisition, E. K. Lee.

References

[1] E. Lee, C. Walde, and B. Mishra, "Effects of cooling rate on precipitate evolution and residual stresses in Al–Si–Mn–Mg casting alloy," Metals and Materials International, vol. 40, no. 4, pp. 815-820, 2018.

[2] I. Jo, C. Ahn, and E. Lee "High-temperature tensile deformation behavior and failure mechanisms of Al-10Si-Mn-Mg high-pressure die-cast alloy," Journal of the Korean Society of Marine Engineering, vol. 43, no. 10, pp. 788-792, 2019.

[3] J. Baskaran, M. Suresh, P. Raghuvaran, V. K. Dharsan, A. Afesul Gayoom, and S. Dharaneetharan, "Mechanical behavior investigation of copper-added A356 alloy," Advances in Materials Research, vol. 5, pp. 853-858, 2021.

[4] M. Mahfoud, A. K. Rao, and D. Emadi, "The role of thermal analysis in detecting impurity levels during aluminum recycling," Journal of Thermal Analysis and Calorimetry, vol. 100, no. 3, pp. 847-851, 2010.

[5] S. Oh and H. Kim, “Effect of scrap addition ratio on tensile and solidification cracking properties of AC4A aluminum casting alloy,” Journal of Korea Foundry Society, vol. 40, no. 3, pp. 85-96, 2020 (in Korean).

[6] H. Soh, “Recycling technologies of aluminum,” Resources Recycling, vol. 28, no. 2, pp. 3-13, 2019 (in Korean).

[7] D. Kim, J. Yoon, C. Choi, S. Choi., M. Hong, S. Shin, and B. Ye, “Changes of microstructures and mechanical properties of recycled AC2B alloy chip fabricated by solution heat treatment.” Journal of Korea Foundry Society, vol. 38, no. 2, pp. 32-40, 2018 (in Korean).

[8] H. Park, H. Lee, and J. Kim, “Preparation of aluminum hydroxide by recycling of aluminum dross,” Journal of the Korean Institute of Resources Recycling, vol. 10, no. 5, pp. 8-15, 2001.

[9] D. Fratila, “Macro-level environmental comparison of near-dry machining and flood machining,” Journal of Cleaner Production, vol. 18, no. 10-11, pp. 1031-1039, 2010.

[10] A. Wagiman, M. S. Mustapa, R. Asmawi, S. Shamsudin, M. A. Lajis, and Y. Mutoh, “A review on direct hot extrusion technique in recycling of aluminium chips,” The International Journal of Advanced Manufacturing Technology, vol. 106, no. 1, pp. 641-653, 2020.

[11] V. C. Venkatesh, D. Q. Zhou, W. Xue, and D. T. Quinto, “A study of chip surface characteristics during the machining of steel,” CIRP Annals, vol. 42, no. 1, pp. 631-636, 1993.

[12] G. Jeong, I. Kim, J. Song, P. Shin, and S. Hong, "Effect of scrap impurities on microstructure and mechanical properties of Zr alloys." Journal of Korea Foundry Society, vol. 36, no. 3, pp. 81-87, 2016 (in Korean).

[13] X. Cao and J. Campbell, “The nucleation of Fe-rich phases on oxide films in Al-11.5Si-0.4Mg cast alloys,” Metallurgical and Materials Transactions A: Physical Metallurgy and Materials Science, vol. 34, no. 7, pp. 1409-1420, 2003.

[14] S. Terzia, A. Taylor, Y. H. Cho, L. Salvo, M. Suéry, E. Boller, and A. K. Dahle, “In situ study of nucleation and growth of the irregular α-Al/β-Al5FeSi eutectic by 3-D synchrotron X-ray microtomography,” Acta Materialia, vol. 58, no. 16, pp. 5370-5380, 2010.

[15] A. Ahmadpour, R. Raiszadeh, and H. Doostmohammadi, “Effect of stirring on behaviour of double oxide film defects in A356 aluminium melt,” International Journal of Cast Metals Research, vol. 27, no. 4, pp. 221-229, 2014.

[16] E. A. Mørtsell, F. Qian, C. D. Marioara, and Y. Li, “Precipitation in an A356 foundry alloy with Cu additions-A transmission electron microscopy study,” Journal of Alloys and Compounds, vol. 785, pp. 1106-1114, 2019.

[17] M. Colombo and E. Gariboldi. “Prediction of the yield strength and microstructure of a cast Al-Si-Mg alloy by means of physically-based models,” La Metallurgia Italiana, vol. 109, pp. 5-14, 2017.

[18] S. Roy, L. f. Aallard, A. Rodriguez, T. R. Watkins, and A. Shyam, “Comparative evaluation of cast aluminum alloys for automotive cylinder heads: Part I-Microstructure evolution,” Metallurgical and Materials Transactions A, vol. 48, no. 5, pp. 2529-2542, 2017.

[19] D. Dispinar, S. Akhtar, A. Nordmark, M. D. Sabatino, and L. Arnberg, “Degassing, hydrogen and porosity phenomena in A356,” Materials Science and Engineering: A, vol. 527, no. 16-17, pp. 3719-3725, 2010.

[20] Z. Li, Y. Jing, H. Guo, X. Sun, K. Yu, A. Yu, X. Jiang, and X. J. Yang, “Study of 3D pores and its relationship with crack initiation factors of aluminum alloy die castings,” Metallurgical and Materials Transactions B, vol. 50, no. 3, pp. 1204-1212, 2019.

[21] M. Aryafar, R. Raiszadeh, and A. Shalbafzadeh, “Healing of double oxide film defects in A356 aluminium melt,” Journal of Materials Science, vol. 45, no. 11, pp. 3041-3051, 2010.

[22] X. Dai, X. Yang, J. Campbell, and J. Wood. "Effects of runner system design on the mechanical strength of Al–7Si–Mg alloy castings,” Materials Science and Engineering: A, vol. 354, no. 1-2, pp. 315-325, 2003.